2020•2021

Faculteit Industriële ingenieurswetenschappen

master in de industriële wetenschappen: chemie

Masterthesis

Development of ultra-thin CIGS absorber material with alkali treatment for solar cell production

PROMOTOR :

Prof. dr. Bart VERMANG

BEGELEIDER :

De heer Thierry KOHL

Stijn Driessen

Scriptie ingediend tot het behalen van de graad van master in de industriële wetenschappen: chemie

Gezamenlijke opleiding UHasselt en KU Leuven

UHASSELT KU LEUVEN

UHASSELT KU LEUVEN

2020•2021

Faculteit Industriële ingenieurswetenschappen

master in de industriële wetenschappen: chemie

Masterthesis

Development of ultra-thin CIGS absorber material with alkali treatment for solar cell production

PROMOTOR :

Prof. dr. Bart VERMANG

BEGELEIDER :

De heer Thierry KOHL

Stijn Driessen

Scriptie ingediend tot het behalen van de graad van master in de industriële wetenschappen: chemie

UHASSELT KU LEUVEN

Foreword

With this thesis being the endpoint of my master's degree, I would like to take this opportunity to express my deepest gratitude to everyone who helped me or was involved in carrying out this research. First and foremost, I would like to thank Kohl Thierry for sharing his knowledge about this topic and introducing me to a professional scientific atmosphere. Helping me throughout this project and providing his feedback whenever asked. I would like to thank Prof. dr. Bart Vermang for sharing his extensive knowledge on the topic and enhancing my view on the different aspects of academic research. Also, I sincerely want to thank all the members of the ATFPV research team at Energy Ville, imec, Belgium for their support and feedback on this project. I would also like to thank imec directly for being transparent during the Covid-19 pandemic, allowing me to continue my research with one day of lab access per week. This granted me valuable time to still investigate the topic at hand practically and not bind myself with only theoretical research.

I would like to thank all my teachers at the University of Hasselt for providing me with the opportunity to work on this topic. Teaching me all the basic and specific aspects of what it means to work as a researcher in the field of chemical engineering.

Finally, I would like to express gratitude to all my family and friends for supporting me daily and elevating me to the position I am today.

Genk, 19th February 2021

Driessen Stijn

Contents

List of tables

List of figures

Abbreviations

Acronym	Description
BIPV	Building Integrated Photovoltaic
CBD	Chemical Bath Deposition
CIGS	$Cu(In,Ga)Se_2$
EDS	Energy-dispersive X-ray Spectroscopy
EQE	External Quantum Efficiency
IV	Current Voltage Measurement
PDT	Post Deposition Treatment
PL	Photoluminescence
PV	Photovoltaic
SEM	Scanning Electron Microscopy
SLG	Soda Lime Glass
TCO	Transparent Conductive Oxide
TF	Thin Film

Abstract

As a thin-film photovoltaic technology, $Cu(In,Ga)Se_2$ (CIGS) is gaining popularity in recent years due to increasing efficiencies and fast-growing market prospects. The incorporation of alkali elements such as Na, K, Rb, and Cs into CIGS absorber layers is one of the techniques used for enhancing photovoltaic efficiencies. However, easily reproducible methodologies for this addition are still under investigation. To date, it has been reported that with alkali atom post-deposition treatment (PDT), solar cell characteristics can be improved in terms of Voc, Fill Factor, and thus overall efficiency. In this work, selenization parameters are discussed for the creation of a baseline and co-evaporated CIGS samples are enhanced using post-deposition treatments with fluoride and chloride alkali salt. The PDT is designed as an easily reproducible enhancement using a spin coater and heat treatment. Results of baseline experiments are evaluated using SEM/EDS, PL, and Current-Voltage measurements. For the selenization baseline, higher annealing temperatures resulted in increased solar cell performance and the added pre-annealing step with N_2 caused a homogenization of the CIGS surface. PL-data from the alkali PDT experiments suggest improvements in the CIGS absorber quality, with increased PL intensity measured for larger alkali atoms. SEM images reveal alkali crystal structures for Li, Na, and K, which could be useful for the creation of openings in oxide layers when developing CIGS/CdS front passivation.

Abstract in Dutch

De dunne-film fotovoltaïsche technologie Cu(In,Ga)Se2 (CIGS) wint de laatste jaren populariteit door toenemende efficiëntie en snelgroeiende marktvooruitzichten. Integratie van alkali-elementen zoals Na, K, Rb en Cs in de CIGS-absorber laag is één van de technieken die consistent gebruikt wordt om de fotovoltaïsche efficiëntie van deze cellen te verbeteren. Er wordt echter nog steeds onderzoek uitgevoerd naar gemakkelijk reproduceerbare methoden voor deze toepassing. In dit werk worden selenisatie- parameters besproken voor het creëren van een baseline en worden co-evaporated CIGS-samples verbeterd met behulp van alkali fluoride en chloride via een post-deposition treatment (PDT). De PDT is ontworpen als een gemakkelijk reproduceerbare toepassing door gebruik te maken van een spin coater in combinatie met een warmtebehandeling. De resultaten van de basisexperimenten worden geëvalueerd met behulp van SEM/EDS, PL en IV-metingen. Voor de selenisatie baseline resulteerde hogere selenisatie temperaturen in een verhoogde prestatie van de zonnecel en de toegevoegde pre-annealing stap met N_2 veroorzaakte een homogenisering van het CIGS-oppervlak. PL-gegevens van de alkali PDT-experimenten suggereren verbeteringen in de CIGS absorber kwaliteit, met een verhoogde PL-intensiteit gemeten voor grotere alkali-atomen. SEM-beelden onthullen alkalikristalstructuren voor Li, Na en K, die nuttig zouden kunnen zijn voor het maken van openingen in de oxide laag bij de ontwikkeling van CIGS/CdS front passivering.

Chapter 1

Introduction

With the depletion of natural resources and the demand for electricity increasing year by year, new and existing methods for generating renewable electricity have come to the forefront. Sources like water, wind, tidal wave, or biogas have formed a portion of the energy solution and are continuously improved to increase their efficiency. However, in comparison to these methods, solar energy is considered the most effective solution because of its availability and abundance. For example, in the year 2020 photovoltaic is reported to cover 40% of the total electrical capacity of renewable energy sources in Germany [1] (see Figure 1). In order to keep solar energy viable, it will need to compete against conventional energy sources. To ensure this, cost-effective reproducibility and reliable fabrication methods will need to be established to deliver efficient functioning solar cells.

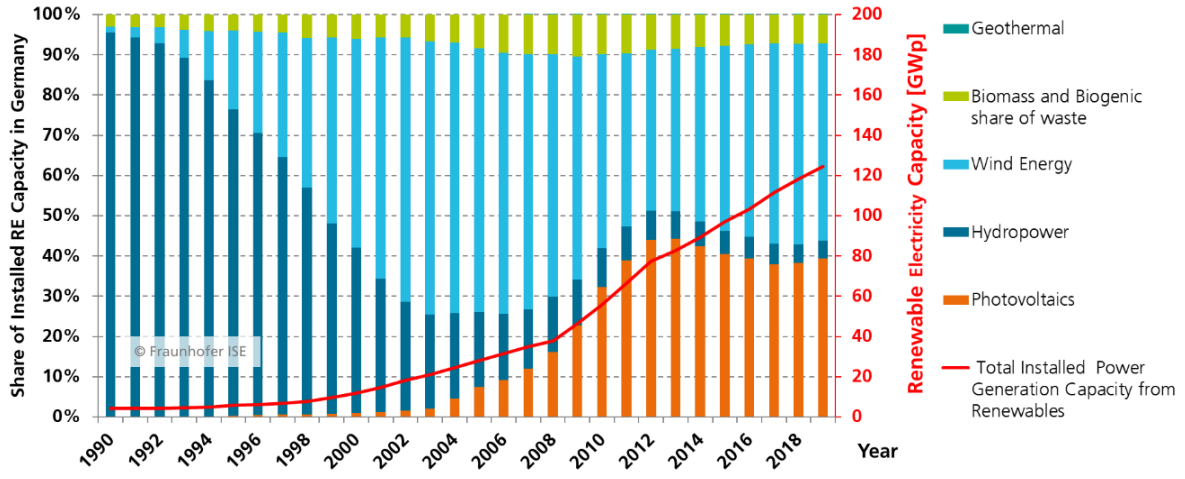

Figure 1 Electrical Capacity of Renewable Energy Sources Germany [1, p.18]

For the photovoltaic industry, Figure 2 shows that the material of choice is typically crystalline silicon (c-Si), with a global market share of 95%. It is still considered to be the most reliable material for fabrication because Si is highly available in nature. However, the problem with Si-based solar cells is that it requires an energy-intensive process for its purification and crystallization, and its installation requires heavy glass protection [2]. This makes thin-film technologies a topic of interest due to their potential lighter weight, lower cost, and substrate flexibility. Thin-film solar cells for example are ideal for more refined applications such as building-integrated PV (BIPV). Currently, three inorganic thin film technologies compete in the photovoltaic market. Namely amorphous hydrogen alloyed (a-)Si:H, polycrystalline heterojunction systems CdS/CdTe, and CdS/$CuInSe_2$. CIGS tends to present the highest efficiency potential of the three inorganic thin-film technologies with reported record lab cell efficiencies of 23.4% [1]. Chalcopyrite based solar cells are capable of such efficiencies due to their direct bandgap, which leads to a higher light absorption coefficient and allows for an overall lower thickness compared to the more traditional silicon-based PV technologies. The higher light absorption coefficient is important because it allows CIGS to be more efficient in terms of photons absorbed per area of absorber material used.

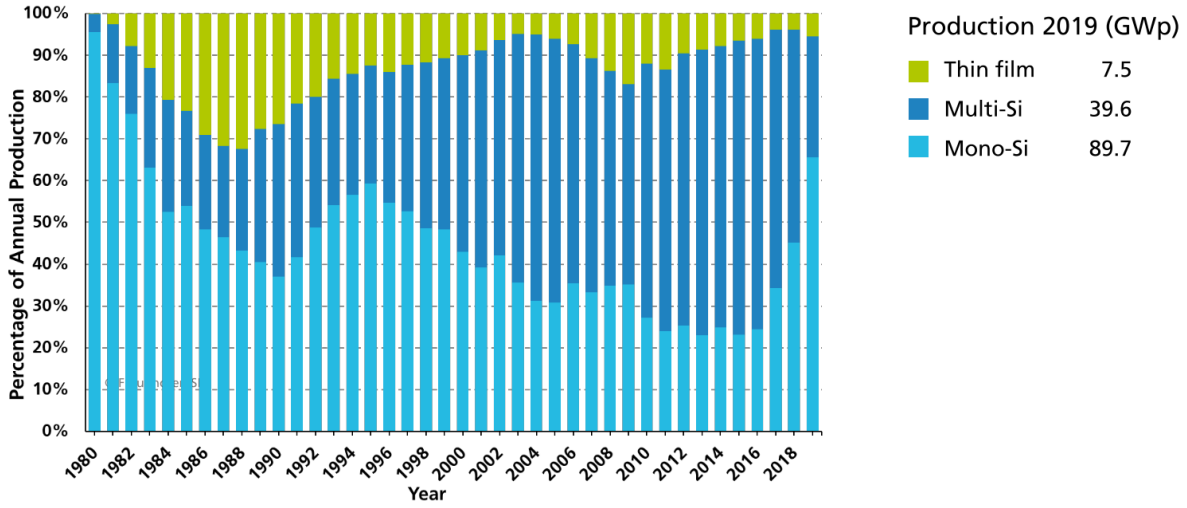

Figure 2 Percentage of Global Annual Production [1, p.21]

CIGS absorber layers are most commonly created by preparation methods such as co-evaporation processes or selenization techniques. While co-evaporation has yielded the highest efficiencies for a long time, the large commercial manufacturers of CIGS reported record efficiencies using a sputtered precursor with subsequent selenization and sulfurization, the so-called two-step process. This technique allows the industry to treat large amounts of precursors at the same time, thus reducing the processing costs [3]. Hence, analyzing the fabrication of the CIGS absorber layer in terms of the selenization parameters is beneficial to the development of the overall CIGS thin-film solar cells.

With the reduction and optimization of the CIGS absorber layer, new aspects of CIGS absorber material construction have come to the forefront. It is reported that the incorporation of alkali atoms into the CIGS structure post-deposition play a critical and necessary role in the development of record efficiency cell. Looking into the composition of a CIGS structure, the four elements Copper, Indium, Gallium, and Selenium are bound to have defects in the crystal formation. Studies have shown that the incorporation of alkali atoms, like Sodium (Na), Potassium (K), Rubidium (Rb), and Cesium (Cs) into the structure of CIGS is beneficial to the optical and electrical properties of the cell [3],[4],[5][6]. For industry scale, post-deposition treatments (PDT) of alkali elements is usually done by means of evaporation [7]. The alkali salt solutions are heat treated in a vacuum after or alongside the co-evaporation of the absorber layer. This makes it ideal for industry because this way the process is easily automatized and controlled. In terms of lab-scale PDT, spin coating of alkali salt solutions onto finished absorber layers can be a cheap and reliable way of processing.

Derived from the arguments mentioned above, the goal of this work is to fabricate CIGS absorber layers with the help of selenization techniques and improve the electrical and optical characteristics of these layers with the incorporation of alkali elements via post-deposition treatments. In Chapter 2, a summary of the structure of a typical CIGS solar cell is presented, alongside the techniques used for creating and characterizing these absorber layers. The methods for enhancing the absorber layer with alkali elements using PDT will also be discussed here. Chapter 3 will focus on the results of the experiments described in the previous chapter and summarize the most interesting aspects. Finally, in Chapter 4 a conclusion of all the gathered results is discussed.

Chapter 2

Experimental Methods

2.1 CIGS-based solar cells

2.1.1 Glass substrate

Thin-film solar cells are generally developed on substrates made of glass, polymers, or stainless steel. The substrate used in this work for creating CIGS solar cells is soda-lime glass (SLG). The reason being that it is relatively cheap, available in a large volume, rather stable over time, and can have several shapes and sizes, in this case, 2,5x5cm. On top of the bare glass, a layer of silicon oxide (Si(O,N)) and molybdenum (Mo) is present, respectively providing the substrate with a diffusion barrier for alkali (see paragraph 2.2.1) and a back contact. Alternatively, glass substrates without alkali elements present, like sapphire or zirconia, can also be used to experiment with the effect of alkali elements [4]. Next, two layers of metals are deposited using sputtering. First, copper and gallium are deposited together in standard conditions of 30°C, whereas the indium layer is sputtered on top of the Cu/Ga layer. The substrate is equipped with a protective barrier and containing the correct metals, the precursor is ready for selenization.

2.1.2 Absorber layer fabrication

The metallic (Cu,Ga)/In precursor is then selenized in an Annealsys AS-One furnace, which allows up to four 5x5cm samples to be processed simultaneously. These samples can be heated in two different positions. The upside-down position, meaning the absorber-layer facing away from the heating lamps, and the upside-up position, with the absorber layer facing towards the heating lamps. This position is reported to have different results because of directly exposing the CIGS layer to the heating lamps [8]. In this research, only one sample was annealed per run, placed in the top left corner of the susceptor, and the upside-down position. Figure 3 shows the Annealsys tool with the most important aspects.

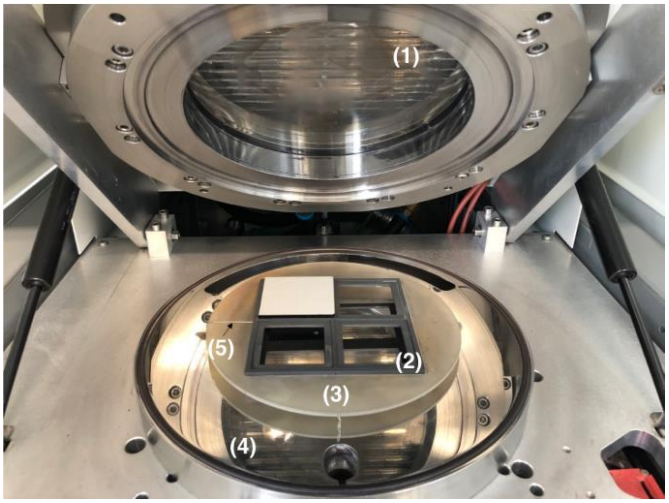

Figure 3 Annealsys AS-one chamber, Lamp furnace (1), graphite susceptor (2), quartz plate (3), bed plate (4) and thermocouple (5) [7, p. 15]

The chamber is equipped with a purge gas line for venting and 4 different process gas lines with mass flow controllers. N_2, H_2, H_2S, and 10% H_2Se diluted in N_2 can be fed into the chamber with gas flows of maximum 2000 sccm (standard cubic centimeters per minute) for N_2 and H_2 and 1000 sccm for H_2S and H_2Se. The recipe is controlled by the user via the Annealsoft software and different process parameters can be altered. Once the sample is loaded into the chamber, the user will need to define a recipe with the specific desirable parameters. The recipe can be downloaded, and the annealing procedure can be launched. A typical CIGS annealing recipe consists of a diverse number of steps which are presented according to the time frame as follows:

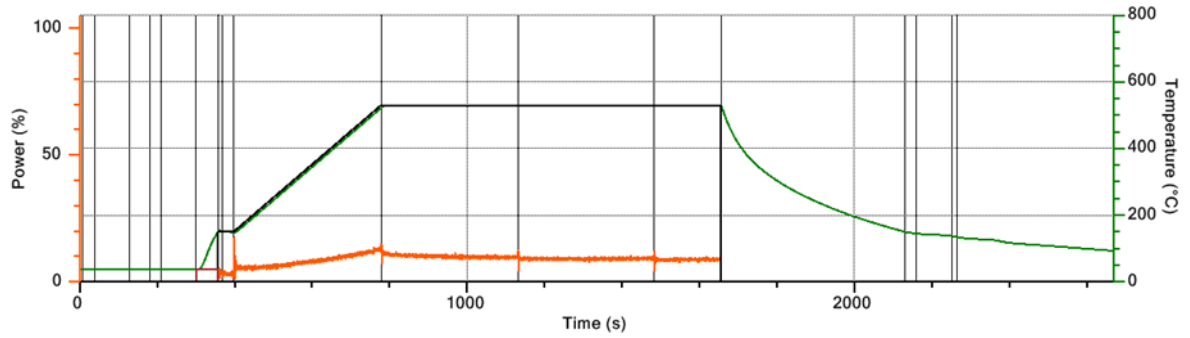

Figure 4 Profile annealing run, power (orange), and temperature (green)

- Venting and pumping: This step is introduced at the beginning of the annealing process and consists of venting the chamber twice with N_2. Thus, allowing the chamber to be cleaned of any gases and particles that might contaminate the upcoming selenization step. During this step, the chamber is controlled at room temperature and put under vacuum conditions in order to be ready for the next heating step.

- Pre-heating: This allows the reaction chamber to achieve an even temperature distribution before it is heated up to selenization temperature. The heating lamps are kept at 4% of their full power to ensure gradual heating. Once a temperature of 150°C is reached, the power stays constant in order to stabilize the temperature in the chamber. If these requirements are met, the recipe will proceed to the next step.

- Ramping: Here the temperature in the reaction chamber is ramped to the final annealing temperature at a fixed rate. The power of the lamps varies in this step to ensure a ramp rate of 1°C/s. Together with the ramping, H_2Se is introduced into the reaction chamber with a constant flow of 20-sccm, to avoid overpressure in the chamber.

- Annealing: Once the annealing temperature is reached, the actual annealing time starts and the H_2Se flow will stay at 20-sccm. With this continuous flow, the reaction chamber will reach its pressure point of 500 mbar in 6 minutes, and thus multiple extra steps of pumping are needed for annealing times greater than 6 minutes. The recipe used in this research allowed the sample to anneal for 15 minutes, meaning three extra steps of pumping were needed.

- Cooling: After the annealing time has expired the power to the heating lamps is set to zero and the system will reset and cool down to below 150 °C. Once at this temperature a standard post-recipe will start purging the reactor. During this step, the reactor goes through one more venting and pumping cycle to ensure the removal of residual gases. Lastly, the sample can be taken out of the reactor and the selenization step is complete.

2.1.3 CdS deposition

After the formation of the absorber layer, cadmium sulfide (CdS) is put on top of the absorber layer to complete the p-n junction of the solar cell and avoid the oxidation of CIGS. The layer is grown by chemical bath deposition and the used solution contains a Cd salt, thiourea as a sulfur source, and ammonia in an aqueous solution. The treated samples are first cleaned with $S(NH_3)_2$ for 30 minutes, dipped in water, and blown dry with a nitrogen pistol. The samples are then attached to a glass holder and lowered into the solution, which is preheated to 60°-80°C. Next, the thiourea will hydrolyze, together with cadmium and sulfur ions to then recombine to from CdS. The layer is then grown in the solution by the combination of two mechanisms, either directly at the substrate or nanoparticles are formed in the solution and will then deposit onto the substrate. The CdS layer is expected to have a thickness of around 50 nm.

2.1.4 TCO and grid deposition

Once the CdS layer is deposited onto the CIGS absorber layer, intrinsic Zinc oxide (i-ZnO) and Tin Oxide (ITO) window layers are used to avoid surface charge recombination. Finally, grids are deposited on the window layer by using a mask and thermal evaporation process. The grids consist of nickel and silver and provide the sample with individual cells. Afterward, lines are scratched onto the sample designating each individual cell for IV-measurement. Lastly, at the side of the sample, a small area is completely scratched away until the Mo back contact and silver are added here to improve the contact resistance.

2.2 Incorporation alkali elements in CIGS-based solar cells

2.2.1 Alkali elements

Solar cells with CIGS-based absorber layers can be improved with the controlled incorporation of alkali metal atoms using post-deposition treatment (PDT). Introducing alkali metals like Li, Na, K, Rb, and Cs have led to record efficiencies of up to 22.9% for thin-film solar cells [3]. The effect of the atoms in the absorber layer has indicated that they may act as impurities or agglomerate into secondary phases and can play a beneficial role in the optical and electrical properties of the solar cell [5]. Specific knowledge of the different effects each alkali metals has can enable further progress, and ultimately give a clearer understanding of what happens at an atomic level and how they are responsible for observed improvements.

Table 1 SLG composition as extracted from [4, p.12]

Compound	SiO_2	Na_2O	CaO	MgO	K_2O	Al_2O_3	SO_3	Fe_2O_3
Composition (at%)	72.20	14.30	6.40	4.30	1.20	1.20	0.03	0.03

Since SLG contains alkali atoms, creating a CIGS-based layer on these substrates in a growth environment temperature of 500°C or higher will lead to alkali atoms diffusing (see Figure 5) into the CIGS absorber layer during the annealing process [9] (see Figure 5). Because of the consensus that these alkali atoms improved the solar cell, the diffusion was not seen as a general problem to fix in early studies. In more recent years, different substrate materials and studies into thicknesses have come to the forefront. Metal and polymer substrates are seeing more applications and with these materials not containing alkali metals to improve the cell, it is becoming more important to understand and quantify the effect of alkali elements in the CIGS absorber layer [9].

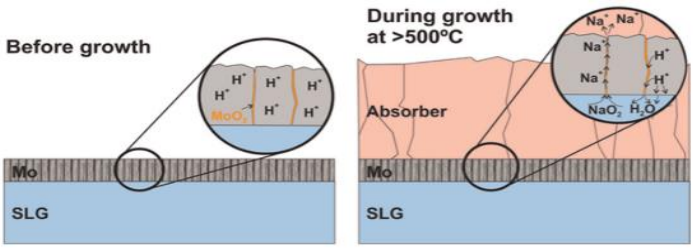

Figure 5 Diffusion of Na from SLG [4, p.13]

For this part of the master's thesis, enhancing the CIGS absorber layer with alkali atoms will be done on thin co-evaporated samples. These 2.5x5cm samples consist of a 1mm SLG substrate base, with on top a Mo layer and an absorber layer (500nm) co-evaporated in a one-stage process. Note that these samples do not contain the silicon diffusion barrier, meaning that during heat treatment alkali atoms present in the SLG can diffuse to the absorber layer. The decision to use these samples was taken externally to ensure quality and a comparable baseline for the alkali PDT. Derived from the arguments in chapter 1, a series of different alkali salts became the subject of the analysis. Table 2 shows all the available alkali salts, alongside their molar mass to calculate the amount of solid powder needed to create solutions of 0,2M. For obtaining comparable results this parameter was fixed. The solutions were created with the help of an analytical balance and an automatic stirrer.

Table 2 Overview of alkali solutions

Concentration 0,2 mol/L Volume 10 mL	Molar mass (g/mol)	Mass (g)
LiF	25,94	0.052
NaF	41,99	0.084
KF	58,10	0.116
RbF	104,47	0.209
CsF	151,90	0.304
LiCl	42,39	0.085
NaCl	58,44	0.117
KCl	74,55	0.149

2.2.2 Post deposition treatment

Once the alkali solution is prepared, the sample chosen for the PDT is cleaned for 5 minutes in ammonia (NH_4OH) (10%) solution. Furthermore, the step is repeated in an aqueous solution and the sample is dried with a nitrogen gun. This etching step is included to remove a possible oxide layer present on top of the CIGS absorber layer. Next, the CIGS sample is placed inside a spin coater and the alkali solution is deposited with a 5ml pipette, completely covering the surface. To form a homogeneous layer the rotation is set at 3000 rpm and the acceleration to 5000 rpm/m, both have been reported to be the experimental standard of the research group. After the thin film of alkali elements is deposited on the CIGS absorber layer, the alkali atoms need to be diffused into the layer for a more effective result. For this purpose, the samples are transported to a PEO-furnace. This tool is used as a powerful multi-purpose fast ramping furnace with gas inlets and outlets, and it will be used to create a neutral atmosphere with N_2 and to promote the diffusion of alkali elements at a temperature of 350°C for 30 minutes. During this procedure a glass sample is used to cover the treated sample, to prevent Se from vaporizing during the heat treatment. When the recipe is complete the samples will continue production to full solar cell as described in 2.1.3 and 2.1.4.

2.3 Absorber layer and solar cell characterization

Before the absorber layer moves to the CdS-step of the solar cell fabrication process, the layer is analyzed with different tools available at Energy CV. The following paragraphs summarize all the techniques used when they are used and what valuable information is concluded from them.

2.3.1 Scanning Electron Microscopy

The SEM, Vega3 by Tescan, will be used to determine the morphology of the absorber films, as well as helping with image-based analysis of all the different samples. An Energy-dispersive X-ray Spectroscopy (EDS) measurement will be conducted alongside the SEM measurements, giving a quantitative idea of Cu, In, Ga, and Se contents in a localized spot on the sample. In terms of the alkali study, the SEM and EDS will be used to evaluate the presence of alkali crystals and possible secondary phases. The micrographs of all samples are analyzed with an acceleration voltage between 15-20 kV, a beam intensity of 7-15, and at magnifications between 1x – 20kx.

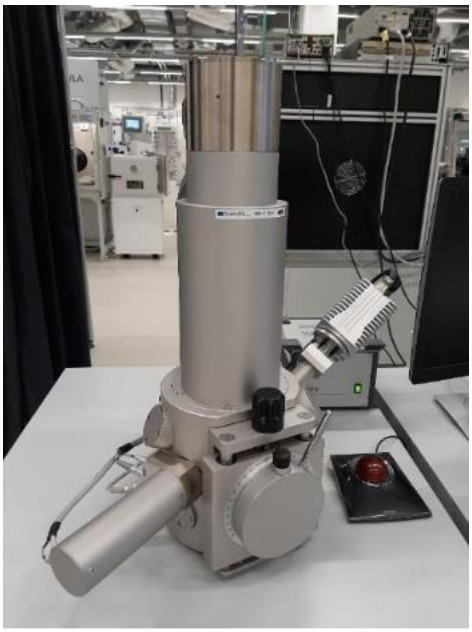

Figure 6 SEM and EDS analysis tool (Tescan Vega 3)

2.3.2 Photoluminescence

The Fluotime300 fluorescence spectrometer by PicoQuant using a high-power He-Ne laser diode will be used to measure the bandgap of the annealed absorber material and the bandgap of the samples treated with the alkali. This bandgap can give an idea of the incorporation of Gallium content into the CIGS structure for the selenized samples and for the alkali study the comparison between different treatments can be analyzed. Also, a lifetime measurement is conducted with this tool to give extra information about the quality of the absorber layer. Several experiments were conducted on different regions of the sample to observe the overall homogeneity.

2.3.3 Current-Voltage Measurement

Current-Voltage measurements are critical when investigating solar cell performance. The electrical parameters, conversion efficiency, open-circuit voltage (Voc), short circuit density (Jsc), fill factor (FF), series resistance (Rs) and shunt resistance (Rsh) can be extracted from measured illuminated and dark J-V curves. All the tests are performed on an oriel solar simulator once the samples are fabricated to full solar cells. The experiment consists of using two needles, one to the silver and the other upon the respective solar cell grid. Measurements are recorded onto a PC initiated through a source-meter. Each cell is measured twice, one for the dark curve and one for the light curve. The electrical response of the cells measured is characterized in the parameters mentioned above.

Figure 7 J-V analysis tool (Oriel setup) at Energy Ville, imec, Belgium

2.3.4 External Quantum Efficiency Measurement

Lastly, external quantum efficiency measurements (EQE) were taken of several samples to better understand the behavior of the cells. A comparison between the ratio of the number of carriers collected by the solar cell to the number of photons of a given energy incident can be made. All these measurements are taken from different alkali samples, to evaluate front, rear surface recombination, and reflection. This data can then give valuable information about the CdS/TCO interface and the range of wavelength absorbed by the CIGS layer.

Chapter 3

Results and Discussion

The main objective of this work is to develop a baseline fabrication methodology for thin CIGS solar cells. Starting with a thin SLG precursor, optimizing the selenization procedure is key for creating a baseline recipe and producing reliable CIGS absorber layers. Following this, the absorber layer is enhanced by a PDT with fluoride and chloride alkali salts. The Results of the various characterization methods that were described in chapter 2 will be discussed in two major sections. First, the results obtained from the selenization experiments, and second the data extracted from the samples treated with the alkali PDT are shown and discussed.

3.1 Selenization series

3.1.1 Baseline annealing step

Temperature is considered to be one of the main aspects affecting the selenization process of a CIGS film [10], [11]. Therefore, the first experiments conducted are to investigate absorber layer behavior on three different selenization temperatures. The baseline CIGS annealing recipes are created following the procedure described in paragraph 2.1, with the chosen selenization temperature of 510/530/550°C. Figure 8 and Figure 9 display the solar cell characteristics, measured with the IV-setup at room temperature. This data suggests a trend in the overall efficiency of the cell, namely that the solar cell characteristics improve with higher selenization temperatures. Considering this is a first iteration of a baseline recipe the efficiency, Voc, Jsc and FF improve form 510°C to 550°C. On the other side the measured resistances also improve, with the series resistance (Rs) decreasing and the shunt resistance (Rsh) increasing with increasing selenization temperature. Rs aims to be as low as possible, considering this resistance can be seen as the overall resistance of the cell. For the Rsh, a higher value is useally more preferd. Low Rsh cause power losses in solar cells by providing an alternative current path for the light-generated current.

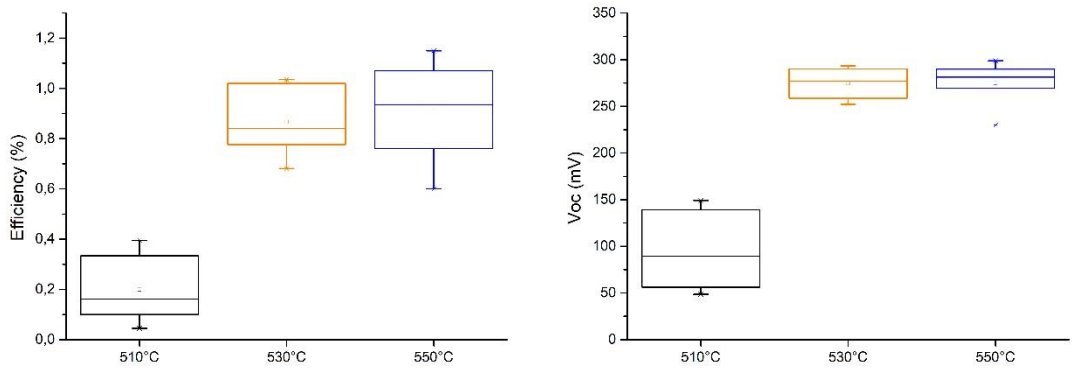

Figure 8 Boxplots: Parameters of the Selenization Temperature series Efficiency and Voc

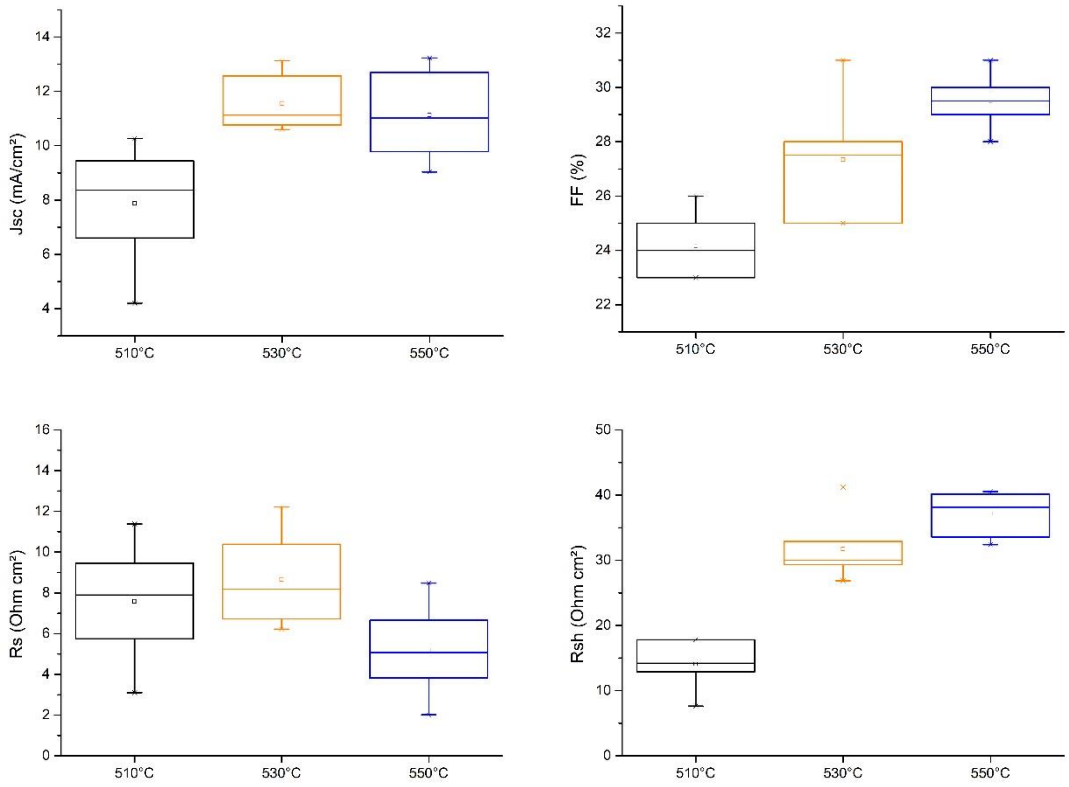

Figure 9 Boxplots: Parameters of the Selenization Temperature series Jsc, FF, Rs and Rsh

One explanation for this change in quality is that with higher annealing temperature a better CIGS phase is formed, thus forming a better absorber layer for the solar cell. Reaction kinetics reveal that the CIS phase (±124 kJ/mol) has lower activation energy than the CIGS phase (144 kJ/mol), resulting in that at lower temperatures the CIS phase preferentially forms. This means when the metals come into contact with Se at the front of the sample, In will predominantly stay at the front, while Cu will diffuse and react with Se to form CIS. Ga for example has to wait longer to react due to the nature of the reaction kinetics and is therefore left at the back to for CGS [12]. It has been reported that Ga accumulating near the Mo back electrode results in lowering conversion efficiency due to a decrease in open-circuit voltage [13]. Thus, a higher temperature, in this case, means more CIGS, due to reaction kinetics and a better intermixing between the CIS and CGS layers. To support this explanation, the amount of Cu, Ga, Se, and In has been measured on the surface of the absorber layer with the EDS. Table 3 shows the atom-% of the absorber layer surface with a clear increase in Ga content present at higher selenization temperatures.

Table 3 EDS-data: CIGS Atom-% on the absorber layer surface and GGI ratio (Ga/Ga+In)

	Cu (%)	Ga (%)	Se (%)	In(%)	GGI
510°C	22.82	2.30	47.94	26.95	0.078
530°C	24.24	2.87	49.95	23.28	0.109
550°C	23.81	3.75	48.52	23.93	0.135

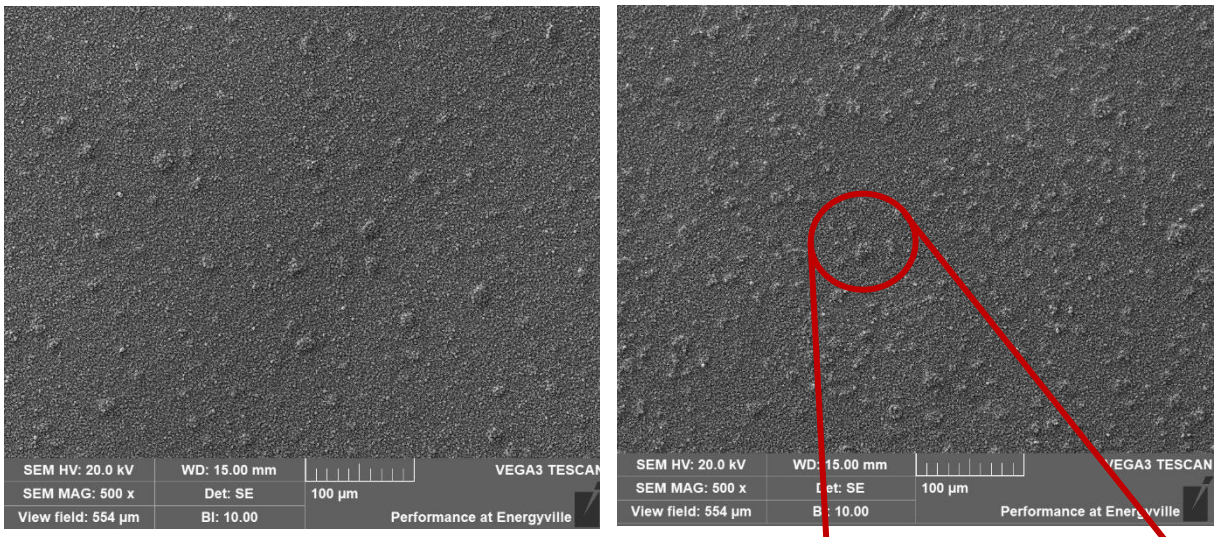

Figure 10 SEM images: Surface of CIGS annealed at 510°C (left) and 550°C (right)

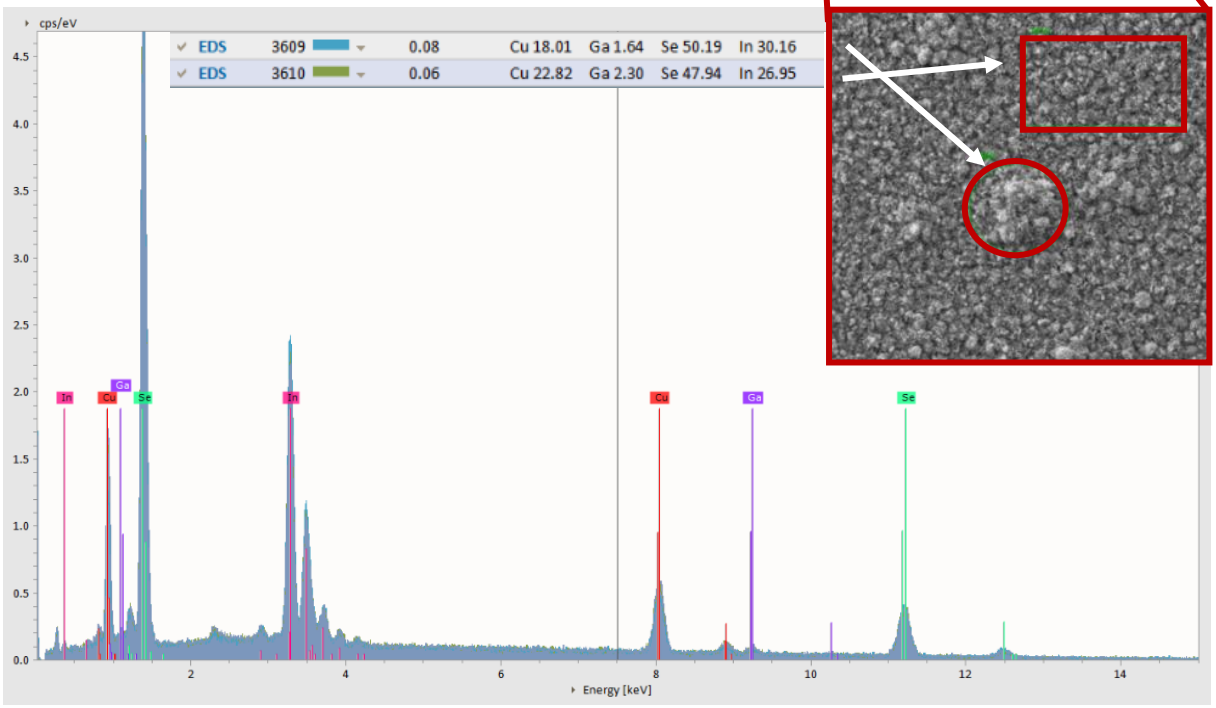

Figure 11 EDS-data: Esprit compact surface scan CIGS surface (3610) and island (3609)

Noticeably, the SEM pictures of each absorber layer showcased a decrease in surface homogeneity, meaning with increasing selenization temperature more agglomerated areas were observed. Figure 10 shows the surface of a sample annealed at 510°C and one annealed at 550°C. EDS data indicated that these agglomerated areas tend to have a larger amount of indium than the rest of the surface (see Figure 11). This observation can be explained as a result of the higher presence of Ga with increased selenization temperature. It has been reported that Ga tends to push out In, causing more concentrated In spots on top of the surface. The cause of this phenomenon starts with the metallic precursors used for the selenization experiments. As reported in chapter 2, these precursors contain a (Cu/Ga) layer, with a In layer sputtered on top. With this fabrication method in mind, it has been reported that In tends to not diffuse well into the other metallic layer and will always behave like a separate layer, resulting in the formation of islands. But on the other hand, one can argue that if the selenization time is increased, and the layers get more time to form the wanted CIGS surface, the agglomerated In islands will disappear and a more homogeneous surface arises.

3.1.2 N_2 pre-annealing step

To promote the diffusion of Ga from the bottom layer to the front, the (Cu/Ga)+In precursor can be pre-annealed in nitrogen atmosphere [13]. This causes the distribution of the metals in the metallic precursor to first homogenize before selenization starts. With this step added, the samples will enter with better and more uniform mixing, namely (Cu/Ga/In) instead of (Cu/Ga)+In. For this reason, the recipe from paragraph 3.1.1 was repeated with an added N_2 pre-annealing step of 7 minutes at 350°C with an N_2 flow of 200 sccm, to avoid oxidation of the elements in the precursor. Figure 12 shows a comparison between the baseline recipe and the recipe used with the added N_2 step.

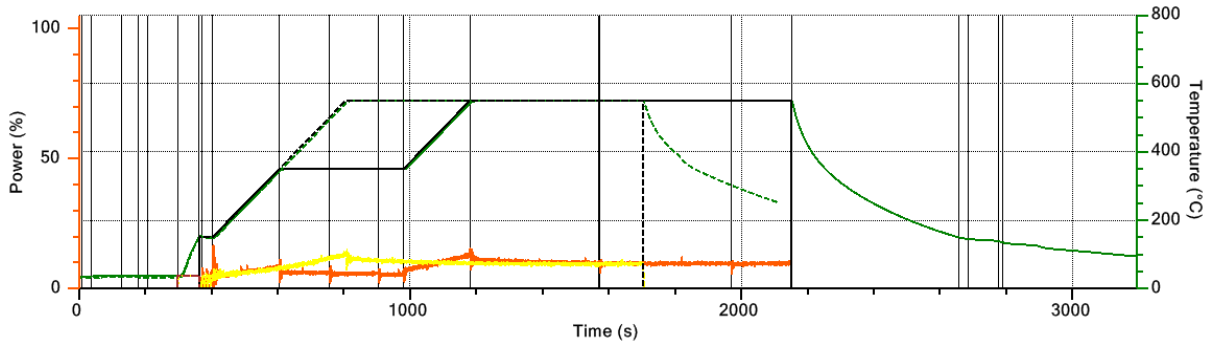

Figure 12 Profile annealing run, baseline recipe (dotted) and baseline recipe + N_2 (solid)

After these samples completed the selenization step, SEM images were taken of the surface to check the effect of the added step. Looking at Figure 13, it is observable that the agglomerated In islands disappeared and as a result, the surface of the CIGS absorber layer is much smoother. Besides, SEM images revealed that the surface for the baseline recipe with added N_2 now contained bigger but less frequent crystal structures. These formations stood out from the regular surface because of their brighter appearance and spiked structure. EDS-data showed these spots contain a higher In fraction than the regular CIGS surface. Thus, when only considering the SEM/EDS data, islands on top of the surface decrease when an N_2 pre-annealing step is added, but less frequent and more concentrated In crystal formation appear. Derived from the arguments above, the conclusion can be made that the addition of the N_2 atmosphere helped metallic precursor mixing to some degree.

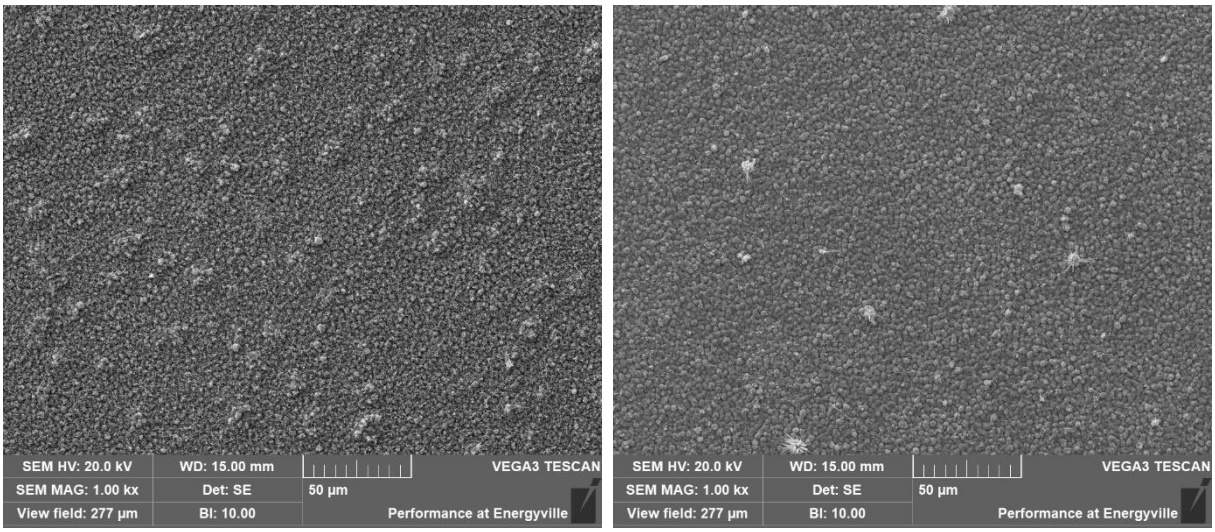

Figure 13 SEM images: Difference in homogeneity (In island formations) for baseline recipe (left) and baseline recipe + N2 step (right)

When higher magnification SEM images are taken from the samples produced in this step, Figure 14 shows that the overall roughness of the CIGS absorber layer chances. With the added N_2 step, the surface tends to not have these needle-like grains and have an overall smoother look. Considering these visual aids from the SEM, one can argue that these absorber layers will achieve a better performance in terms of solar cell characteristics once they have been produced to full cells.

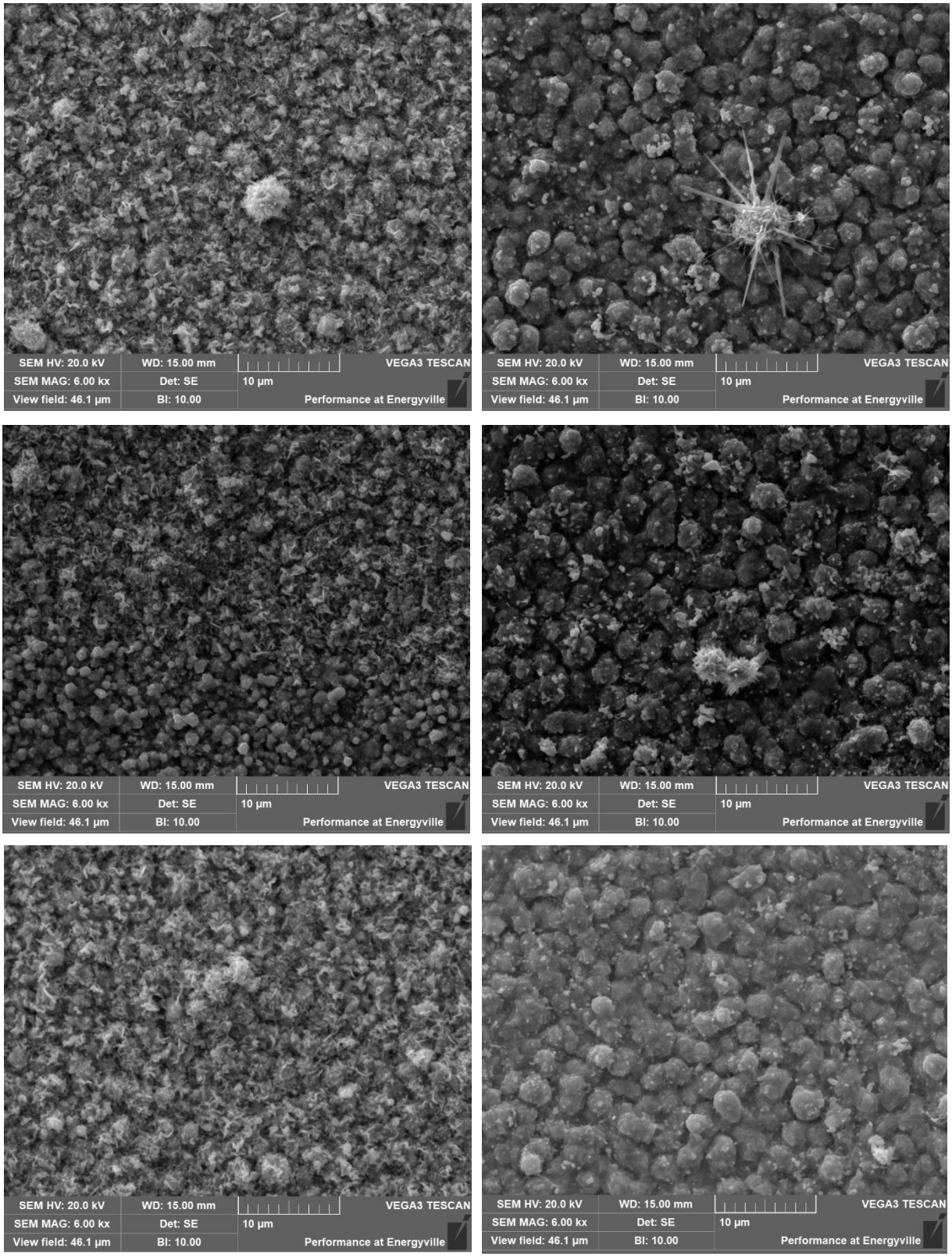

Figure 14 SEM images: Difference in CIGS structure for baseline recipe (left) and baseline recipe + N2 step (right). Selenization temperature 510°C (top), 530°C (middle) and 550°C (bottom)

However, samples produced with the added N_2 pre-annealing step did not yield any results with the standard IV-measurements. For this reason, no IV-data is shown for these experiments. An explanation for the strange behavior of these cells is that the more concentrated secondary phases, In rich crystal structures, developed poor p-n junctions resulting in significant shunt paths.

3.1.3 Intermission: Selenization

This paragraph will serve the purpose of summarizing the observations made for the selenization part of this work and guide the reader towards the next step in enhancing CIGS absorber layers. For the selenization step of the fabrication process, two major aspects were investigated, the selenization temperature and the effect of an N_2 pre-annealing step. Table 4 shows an organized overview of the aspects observed with the selenization experiments.

Table 4 Summary selenization

Temperature experiments:	• IV-measurements revealed higher selenization temperatures resulted in better solar cell performance. 550°C > 530°C > 510°C • This performance was due to better intermixing of Ga into the CIGS surface layer at higher temperatures. • SEM revealed higher selenization temperatures resulted in more In rich secondary phases.
Added N_2 pre-annealing step:	• SEM revealed a decrease in In rich secondary resulting in a smoother CIGS surface. • High concentrated In rich secondary phases present → Possible shunt paths.
Further optimization possibilities:	• Annealing time • H_2Se flow characterization

Due to external decisions, the experiments on the selenization part were put on hold to focus on the alkali PDT part of this master's thesis. In a perfect world, the optimized CIGS absorber layer would go through a PDT with alkali elements to enhance its electrical and optical performance. To ensure continuity and the ability to compare experiments, the precursors were changed to samples with a complete co-evaporated CIGS layer.

3.2 Alkali series

3.2.1 Comparison XF

According to the literature, NaF and KF PDT are generally used when enhancing CIGS absorber layers in terms of electrical performance [5],[14],[15]. Improved Voc and FF values can be obtained when treating the absorber layer with an alkali PDT. For this reason, the first experiments conducted involve the PDT of co-evaporated CIGS samples with fluoride alkali compounds. The chosen fluorides range from LiF to CsF, all treated as described in paragraph 2.2. IV-measurement results in terms of efficiency, Voc, Jsc, and FF are shown in Figure 15. Looking at this data, it is apparent that the overall efficiency of the CIGS solar cell tends to decrease in comparison to the reference cell. With the efficiency stabilizing back to the range of the reference cell with increased alkali size. When the alkali PDT data is compared to each other, so without the reference, a clear trend of improvement can be seen. Ranging from the worst overall performance of LiF PDT to an increasingly better performance with increased alkali size. One of the reasons found in the literature explaining the enhancement of absorber layers with alkali elements is that the alkali atoms tend to fill up holes or imperfections of the complex CIGS structure [16],[17]. This can give a fraction of the explanation regarding the better performance of Cs in comparison to the much smaller atom of Li. Another explanation given in combination with the previous one is that the incorporation of alkali atoms into the CIGS structure provides the layer with better conductivity, so meaning a higher value for Jsc should be measured compared to CIGS absorber layers without alkali atoms. To further understand the influence of the alkali elements, other analysis techniques need to be evaluated.

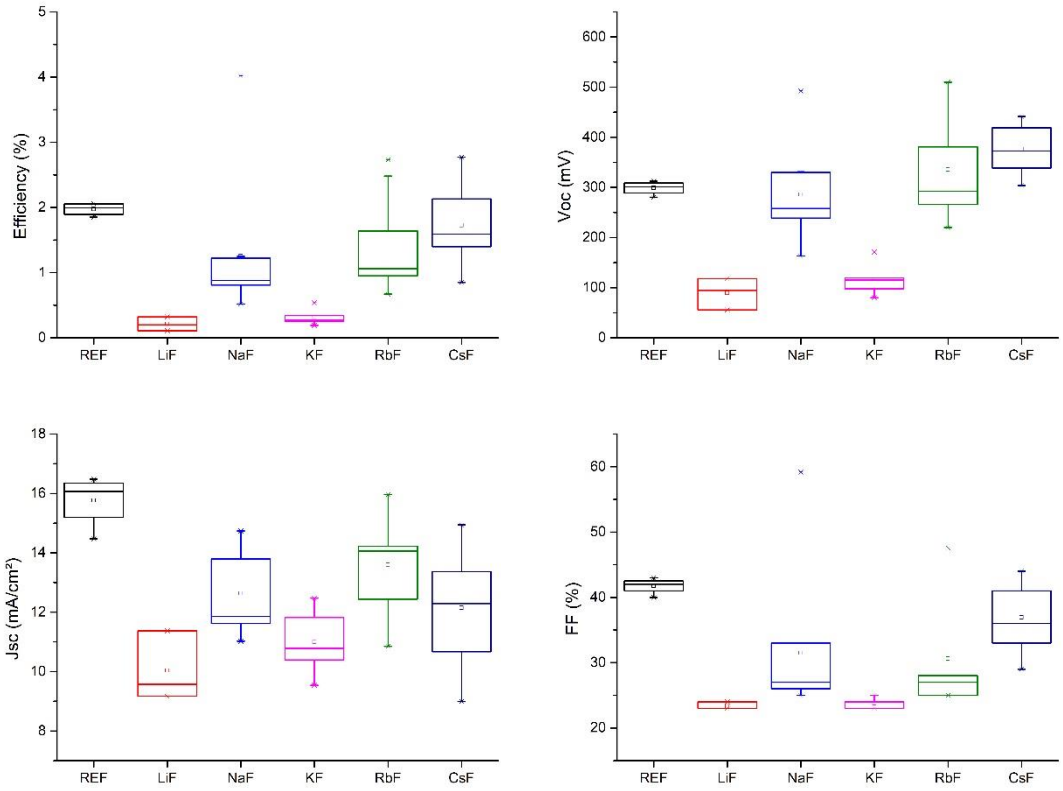

Figure 15 Boxplot: Comparison Efficiency, Voc, Jsc and FF for every XF alkali ranked for small to greater alkali atom size

Looking at the PL results shown in Figure 16, the reference sample with no alkali PDT treatment can be seen at an energy in the range of 1,15 eV – 1,20 eV. Now, one can argue that with every consecutive experiment done with alkali fluorides, the same PL-peak position can be witnessed and an increase in alkali element size shows significantly better peak intensity. This is an important observation because in contrary to the IV-data, this shows that the quality of the absorber layer is improving when treated with alkali elements. For example, when a PL-measurement is conducted a laser will be focused on the surface of the CIGS layer, providing the absorber layer with light photons of a given wavelength (this case 532 nm). Now at the CIGS material bandgap, peak at 1,15-1,20 eV, the material will absorb this energy, and electrons are excited from the conduction to the valence band. Considering electrons do not stay excited for a very long time, they will soon return to their ground state, emitting a photon with the same energy as the one that was absorbed. But in semiconductor materials, it can also happen that an electron from the conduction band recombines with a hole from the semiconductor structure instead of returning to the ground state [18]. This process is called non-radiative recombination and the electron will combine with a hole, resulting in no emitted photon. Now because the PL peak intensity increases with increasing alkali atom size, one can state that the number of photons emitted and measured increases. Meaning, fewer electrons are lost in a non-radiative recombination mechanism and more electrons make the band-to-band recombination, thus meaning more photons emitted. This observation supports the claim that alkali elements incorporated into the CIGS structure fill up vacancies our fault in the crystalline structure and provide better quality. So, the reason that these solar cells are not performing for IV characteristics is not due to the alkali PDT.

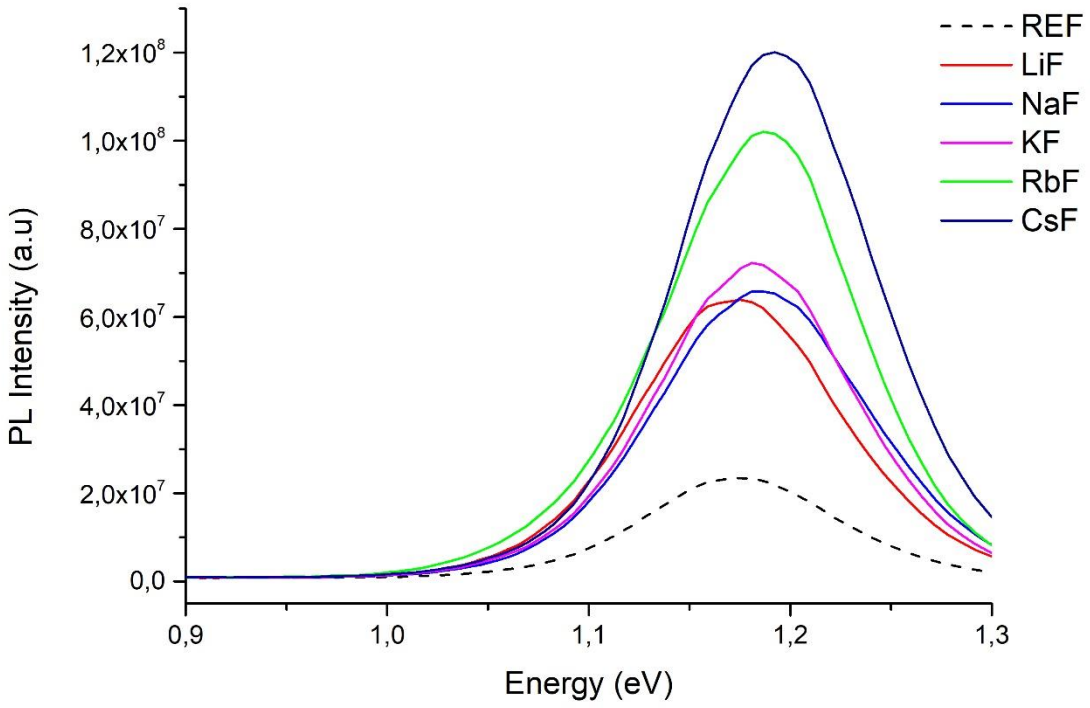

Figure 16 PL-data: Comparison XF and reference sample

Next, the best cells of each alkali sample were conducted through an external quantum efficiency test and the results are shown in Figure 17. This graph plots the ratio of the number of carriers collected by the solar cell to the number of photons of a given energy incident on the solar cell. In this case, the EQE is normalized relative to the maximum EQE value and plotted against the wavelength of the absorbed light. Ideally, the solar cell material would absorb light at every wavelength in the visible spectrum and the graph would appear like a rectangle. For an actual solar cell, the quantum efficiency is reduced due to recombination effects, an overall reduction caused by reflection, and a low diffusion length. At the blue light range (400-525 nm), front surface recombination and CdS/TCO quality are visible because these short wavelengths don't tend to reach deep into the sample layers. Considering this data, NaF seems to have the least parasitic absorption in the CdS/TCO interface. Meaning one can argue that for example, the NaF sample has a thinner Cds layer, a better interface, quality of CdS, or a combination of these aspects. At the right of the EQE peak, these curves have a trend to go downwards due to the thickness of the layer and a low diffusion length, the latter causing recombination. Because of the thin layer, the light will not get the chance to be fully absorbed, resulting in heavier loss with increasing wavelength. In this area, the reference sample tends to perform better than the samples treated with alkali. Which to a degree confirms that the reference samples also score well when looking at IV-data. For Cs, the story is similar because the EQE curve follows the same trends, and in IV CsF was one of the better samples measured. In the case of Rb, relatively good IV results were measured but the EQE curve doesn't show this to the extent of Cs and the reference, pointing to something else happening in the sample. An explanation for this behavior is that Rb has formed secondary phases on top of the CIGS absorber layer, these are stuck between the CIGS and CdS layer, possibly causing reflection in this layer, resulting in a loss of light due to destructive interference [19].

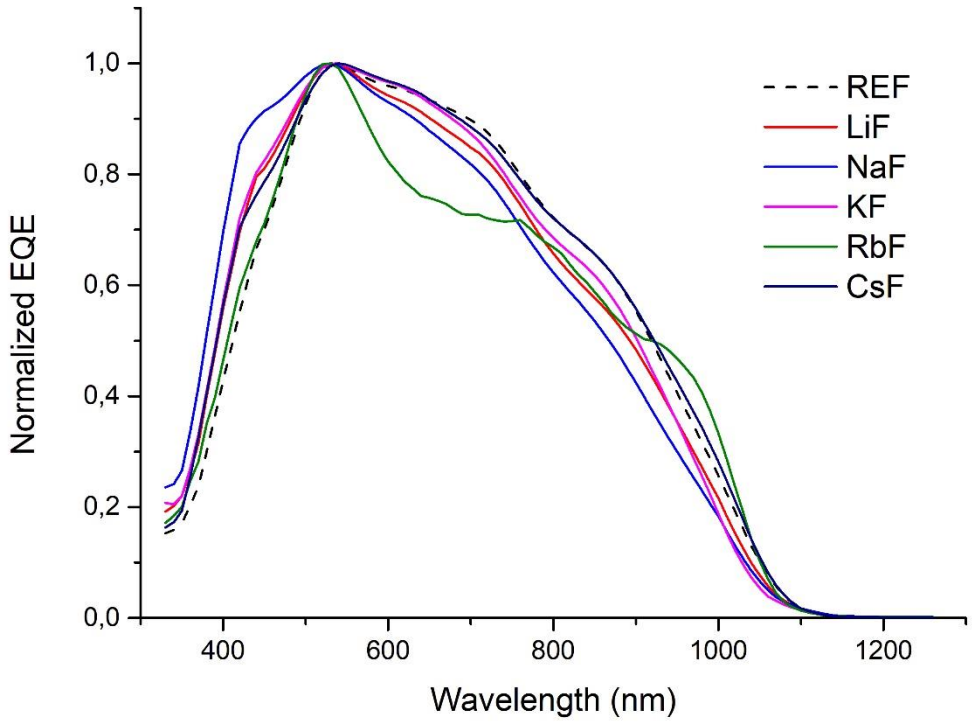

Figure 17 EQE-data: Comparison XF with reference sample

3.2.2 Comparison XF vs XCl

The second series of samples that were investigated are the chlorides. These alkali salts were chosen to form a comparison to the fluoride alkali PDT and see if there are notable differences when XF is changed to XCl. For this reason, the PDT was performed similarly with LiCl, NaCl, and KCl. The same characterization techniques were used, IV-measurements, SEM/EDS, PL, and EQE for evaluating and comparing them to their respective fluorides. Figure 18 shows the results of the IV-measurements made for the chlorides. With a glance at this data, it is apparent that the chloride samples behave in a similar trend to the fluoride ones. Except the chlorides tend to behave better in solar cell characteristics in comparison to their fluoride counterpart. For example, LiCl and KCl perform better in overall solar cell efficiency in comparison to LiF and KF, with NaCl being an exception. Because overall efficiency increases, the other characteristics of the cell increase as well. Improved FF and higher values of Jsc are measured with the chloride samples in comparison to the fluoride ones. The difference in performance can be partially explained by observations made to the alkali crystal structure for each element.

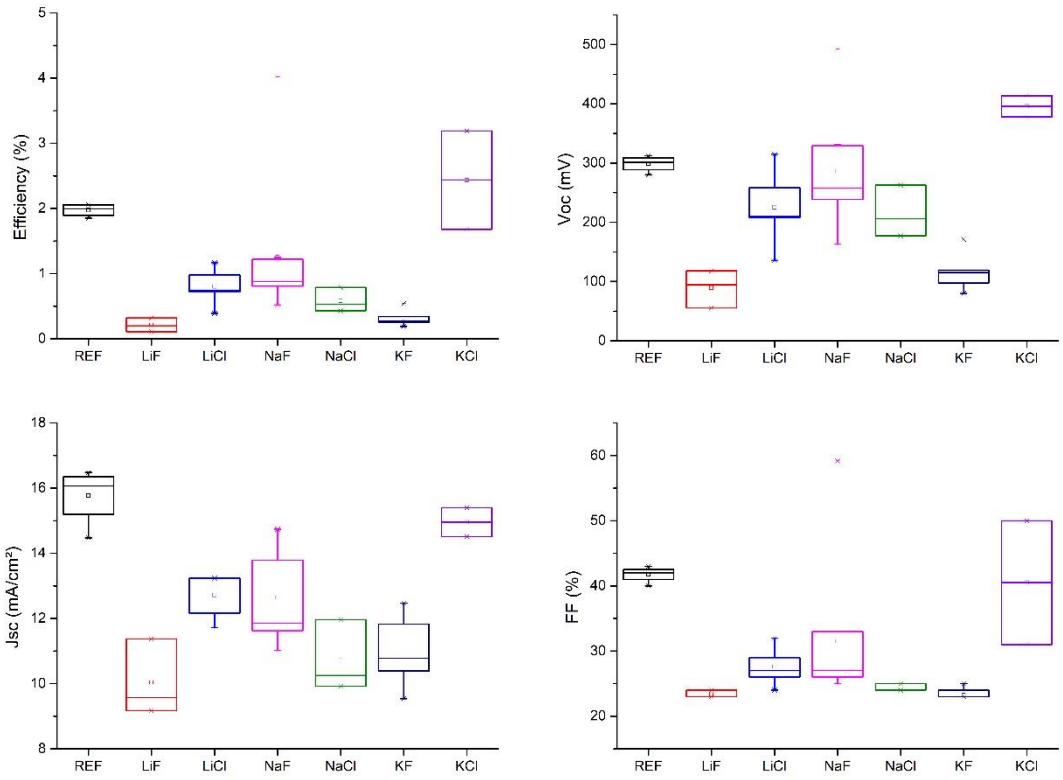

Figure 18 Boxplots: Comparison Efficiency, Voc, Jsc and FF for XF vs XCl

Looking at Figure 19, one can argue that for each different alkali element another crystal growth pattern can be observed. If this data is evaluated in combination with the previously shown IV-data it is apparent that the cells performing well, KCl and to some extent NaF, have a denser alkali crystal layer on top of the CIGS surface in comparison to the other alkali elements. One can argue that this is the result of an excess of alkali in the absorber, and the exceeding atoms are forming crystals on the surface. On the other hand, the amount of alkali on the surface can tell that the diffusion didn't happen properly, and most alkali still resides on top. But according to both IV and PL, KCl and NaF perform best, and they showed a dense crystal structure. Ultimately, this can only tell something about the alkali present in the absorber layer. Once the procedure to full solar cell begins, the alkali crystals will be washed away at the beginning of the CdS step.

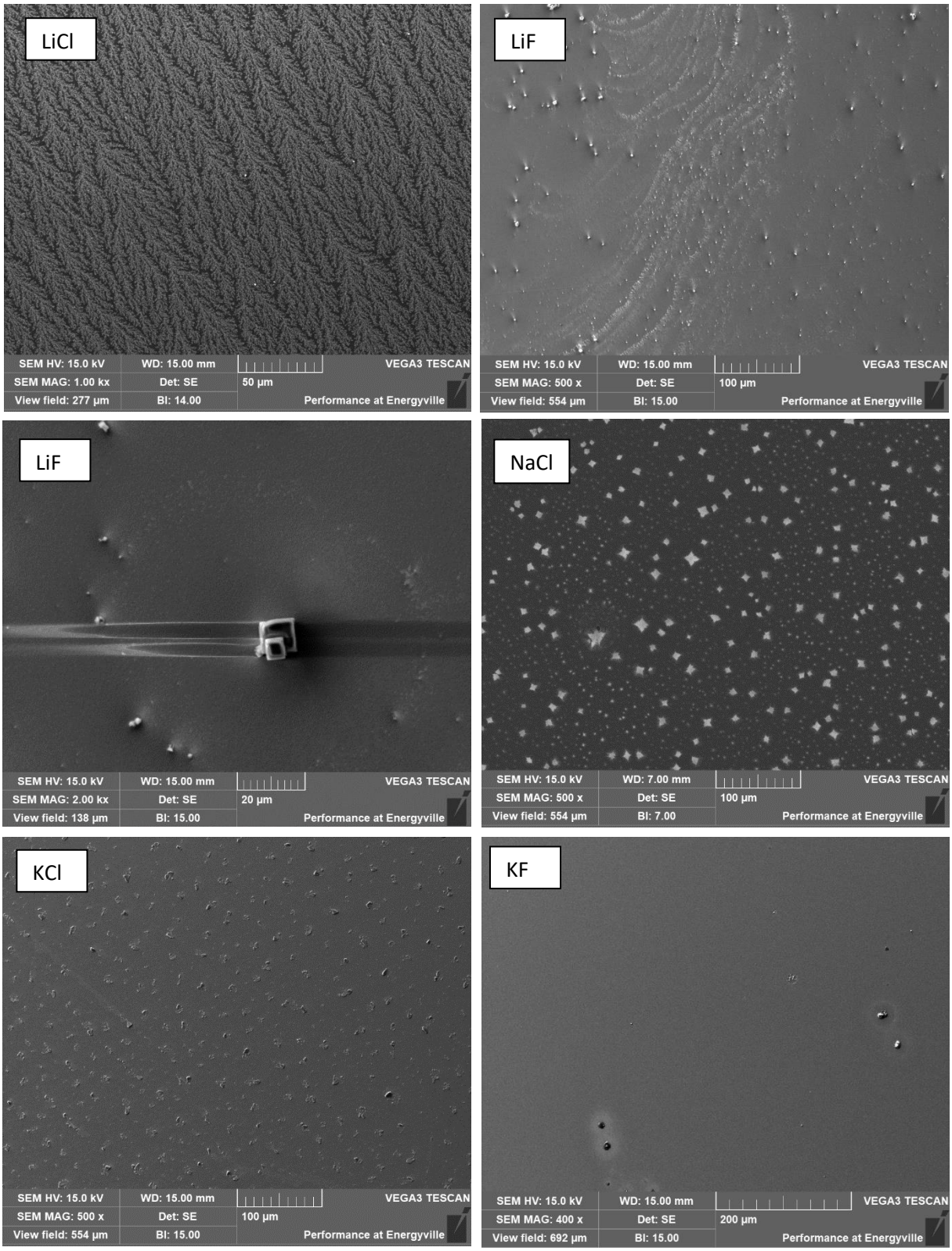

Figure 19 SEM images: Comparison different alkali crystal structures on CIGS surface

Considering the basic PDT used in this work, other interesting aspects of CIGS solar cell development can be studied with the presence of these alkali patterns. For example, in frontal passivation techniques [20], alkali crystals can be used to form small holes in a used oxide (passivator) layer. This provides the solar cell with a layer between the absorber and CdS, which will serve for reducing defects at the CIGS surface but will still provide electrons a route through the set layer without hurting the performance of the cell. So ultimately, the alkali PDT can be used for two major purposes. First, being an enhancement method for CIGS absorber layers, improving CIGS bulk quality and increasing solar performance characteristics. And second, the formation of the alkali crystal on top of the CIGS layer serves a purpose in improving the quality of passivation between bulk and CdS layer, translating in a better p-n junction for the solar cell.

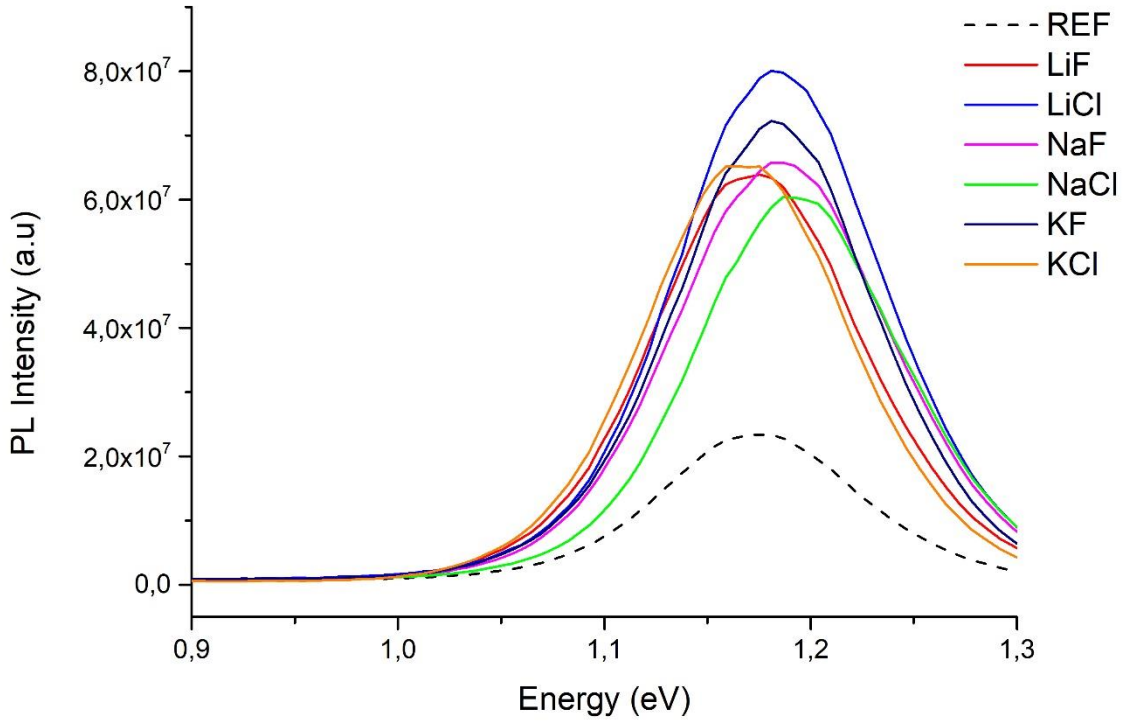

Figure 20 EQE-data: Comparison XF vs XCl

Regarding the PL-data for chloride PDT samples, Figure 20 shows the results in the same manner as previous samples. When comparing the plots of XF against XCl, it is apparent that all chloride alkali PDT had a positive effect on PL intensity. For both NaCl and KCl, characteristics seem to decrease below their fluoride counterpart. The highest PL peak intensity is observed for LiCl, which is contradicting to alkali PDT for the fluorides. Nevertheless, the same global conclusion can be made for this data then the data showed in the previous PL paragraph. According to PL-data, the alkali PDT is improving the quality of the CIGS absorber layer but reviewing IV-data shows that there is something coherently going wrong in other parts of the fabrication to a full solar cell.

EQE-data for the comparison between XF and XCl is shown in Figure 21. Looking at these plots, it can be concluded that Na tends to perform best in the blue range spectrum due to the same reasons mentioned in the XF EQE graph, less parasitic absorption in the TCO and CdS. The other alkali elements tend to perform slightly better in this range compared to the reference sample, meaning that with the alkali PDT the CdS layer arguably gets thinner. In the red area of the EQE curve, KCl seems to outperform the reference sample, verifying a better quality in CIGS bulk. This was also verified by the data gathered for KCl from IV and PL measurements.

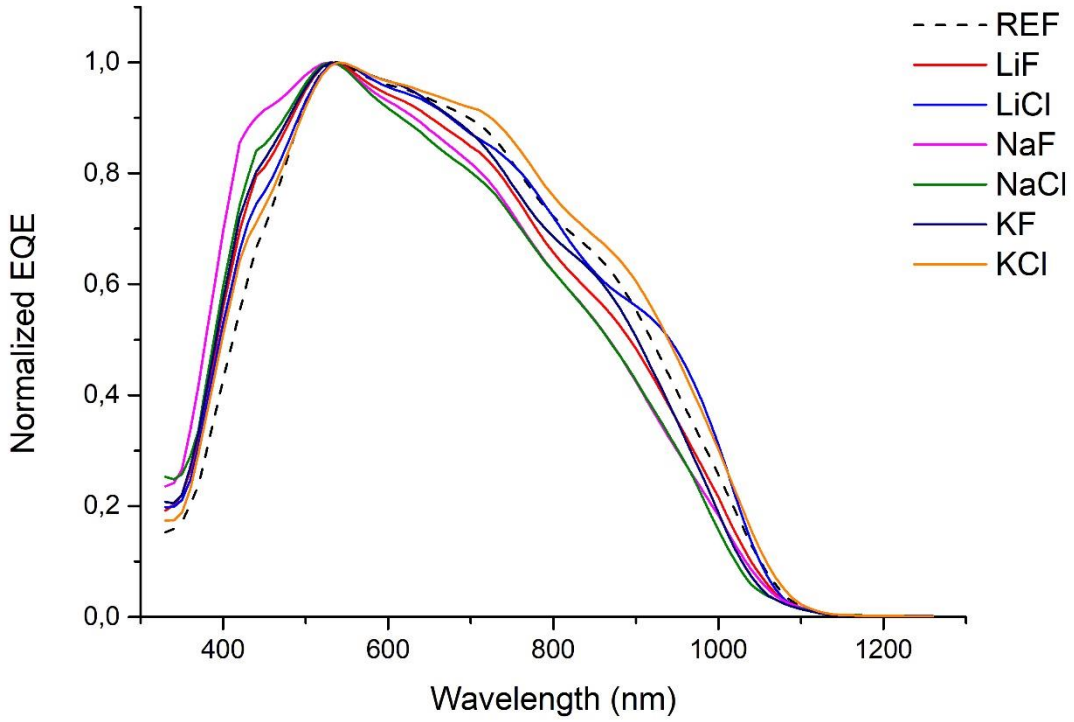

Figure 21 EQE-data: Comparison XF vs XCl

3.2.3 PDT at different temperatures

After the unexpected IV results for the samples treated with alkali PDT, an experiment was conducted to evaluate the influence of furnace temperature during PDT. Once the alkali coat is applied with the spin coating technique, the samples were treated in a PEO furnace, as explained in paragraph 2.2.2. Here a temperature of 350°C was initially chosen to promote alkali diffusion into the CIGS absorber layer. Experience from the research group had shown that this heat treatment temperature may be too high for the sample and could be the problem for the poor IV performance of the cells. This was backed up by the fact that once the alkali PDT was completed, the cell would also be heated for the ITO treatment to a full solar cell. Logically these two heat-intensive procedures could form too much stress on the thin absorber layer and decrease the quality. To investigate this aspect of the fabrication, two KF PDT were carried out following the same steps as usual except one would be heat treated in the PEO furnace at 250°C. Figure 22 shows a summary of the efficiency, Jsc, and PL data measured from these samples. First, it is apparent that decreasing the temperature in the furnace results in better solar cell characteristics as well as CIGS absorber layer quality. Efficiency and Jsc values increased back towards reference standard and PL intensity increased. One can argue that further lowering the temperature could enhance performance, even more, limiting to the point where diffusion aspects would decrease. To ensure these conclusions further experiments need to be carried out to improve this aspect of the PDT.

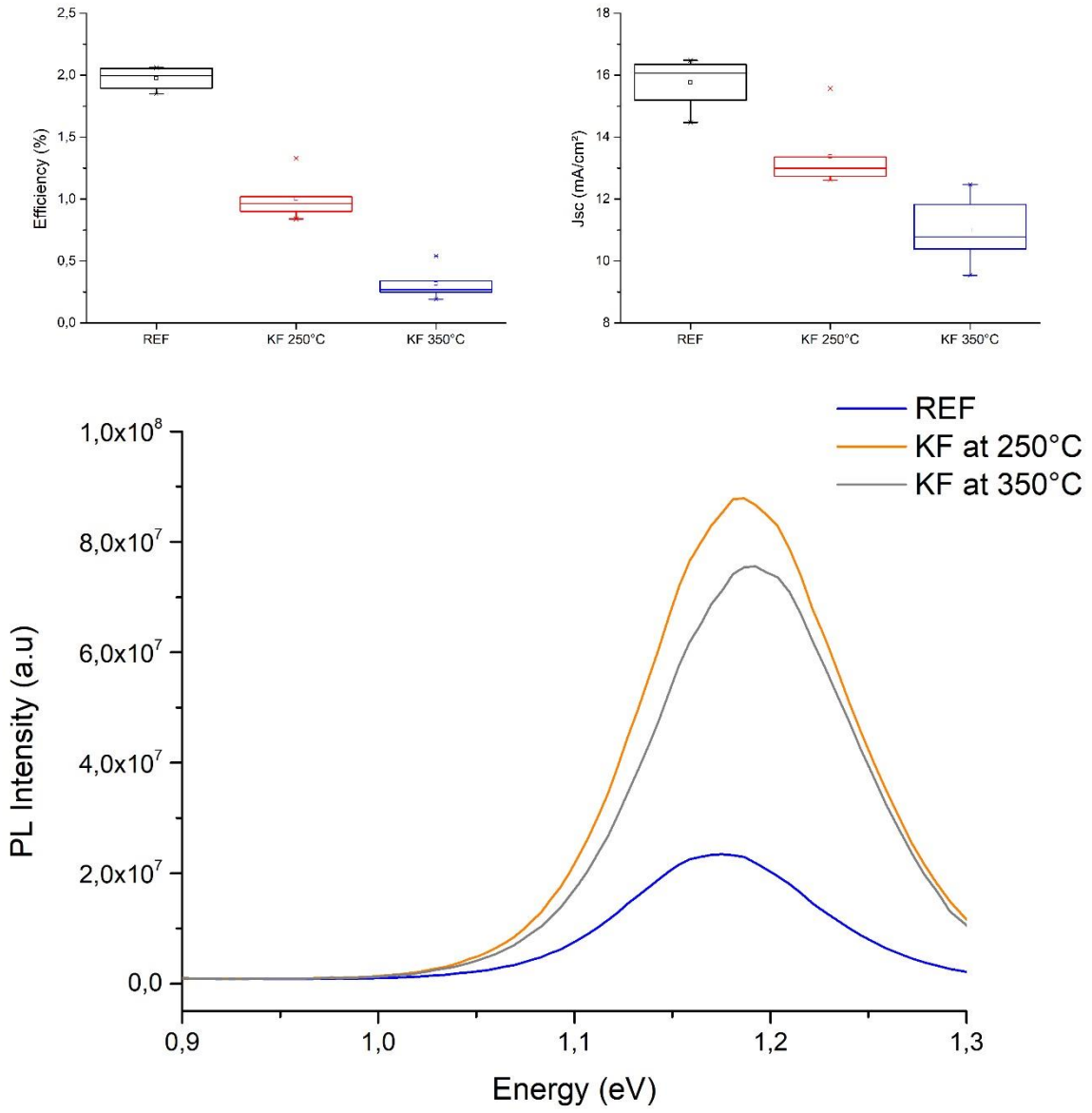

Figure 22 Boxplots + PL-data: Comparison Temperature effect on PDT

Analyzing the temperature dependence further, other researchers recently found evidence that presence of alkali atoms, CdS degrades faster in contact with oxygen. Experiments have shown that CIGS solar cells are very susceptible to creating an oxygen layer on top of their CdS layer when entering the TCO deposition. Namely, the researchers realized that before the i-ZnO step of the TCO deposition, there is a prolonged period where the CdS layer is exposed to an excess of oxygen. This causes the sample to create an unwanted oxygen layer considering the sample is also undergoes increased temperature conditions, which are mandatory for the i-ZnO deposition. Now, it also has been reported by colleague researchers that the formation of the oxygen layer is likely to be promoted when there are alkali elements present in the CIGS sample. Resulting in an isolating oxygen layer between the CdS and i-ZnO layer, presumably decreasing the characteristic of these solar cells significantly and thus creating poor solar cell performance. This is an interesting development in the fabrication methods of the CIGS solar cell because in this work all the alkali-treated samples went through this method of depositing i-ZnO. Presumably being one of the main aspects for clarifying the unexpected performance of the solar cell at IV level.

Chapter 4

Conclusion and Perspective

To finalize the master's thesis, this paragraph will consist of a summary of all the observations and conclusions made for both the selenization and alkali PDT part. In a perfect experimental environment, the alkali PDT would begin after a full optimization of the CIGS absorber layer. But due to external decisions and limited time, the selenization experiments were only analyzed in terms of annealing temperature and the effect of an N_2 pre-annealing step. Instead, the major focus was set on improving co-evaporated CIGS absorber layers with alkali fluorides and chlorides. Within mind, developing a strong and reproducible baseline using a spin-coater and heat treatment for the addition of Li, Na, K, Rb, and Cs into this absorber layer.

For the selenization part, IV-data showed an increase in solar cell characteristics with higher selenization temperatures. This meant that among 510/530/550°C, the latter showed the best values for Voc, FF, and thus overall solar cell efficiency. With this increase in temperature, SEM images suggested an increase in the concentration of In-rich islands on the CIGS surface. On closer inspection with the EDS tool, both phenomena could be explained by surface composition and reaction kinetics. An increased selenization temperature favored the reaction kinetics of CIGS over CIS, meaning that at a higher temperature more CIGS phase was formed, and a better intermixing took place between CIS and CGS. This then resulted in more Ga at the front of the absorber layer, explaining the improved solar cell performance. Alongside this increase of Ga at the front, In tended to concentrate in more localized islands changing the CIGS surface morphology. An N_2 pre-annealing step was then added for promoting the diffusion of Ga further, by trying to homogenize the metallic precursor before annealing. This way the three metals inside the precursor could behave like one (Cu/In/Ga) layer and not the expected (Cu+Ga)/In. SEM images from these experiment runs showed a decrease in the In islands in combination with a smoother CIGS surface. This meant that to some extent a better intermixing of the four elements took place and one could assume an improved quality of CIGS bulk. However, IV data suggested that with the addition of this pre-annealing step, significant shunt paths had developed due to the formation of In bulbs on top of the CIGS, resulting in very poor IV performance.

The alkali PDT resulted in creating an improved quality of CIGS bulk, with higher PL intensities measured for the sample treated with larger alkali atom size. This means that for all the fluorides, CsF showed the highest PL intensity, suggesting that Cs reduced non-radiative recombination possibilities inside the CIGS bulk in comparison to the reference sample. In terms of the difference in fluoride or chloride alkali salt performance, no concise conclusions can be made with the completed experiments. An interesting aspect discovered with the alkali PDT experiments was the difference in the performance of the cell at PL and IV levels. The fact that PL-data suggested improved CIGS layer quality, but IV results were below expectations indicated that to some extent the poor performance of the cell had nothing to do with the alkali PDT. Further into the developing process it was discovered by colleague researchers that an unwanted oxide layer formed between the CdS and i-ZnO layer during the fabrication to a full solar cell. Presumably, because during the preparation of the i-ZnO step the sample is exposed to an excess amount of oxygen in combination with an increase in temperature. In addition to this, it was reported that samples treated with alkali PDT were more vulnerable to the creation of the oxide layer, resulting in an unwanted layer hurting the performance of the cell and being the main reason for the poor IV performance measured for the samples in this work.

With the completion of these experiments, new research questions and possibilities arise for the selenization and the alkali PDT. In order to further optimize the process of selenization, future work could focus on the annealing time and H_2Se flow in different steps of the process. Annealing time is briefly mentioned in this work because, in combination with selenization temperature, these two process parameters are key to obtaining reproducible CIGS absorber layers. One could also investigate the effect of increased H_2Se flow during ramping and annealing and seeking the advantages when increasing the supply of Se. In terms of the alkali PDT, an interesting possibility arose with the observation of clear alkali crystal structures on top of the CIGS layer. These crystals could be studied and grown in sizes useful for front passivation of the solar cell. The PDT could ultimately be optimized to provide the cell with an enhancement in CIGS bulk for better solar cell performance and the crystals grown as a side effect of the PDT could then be used for creating reliable paths through the passivation layer when developing this front passivation.

References

[1] FRAUNHOFER INSTITUTE FOR SOLAR ENERGY SYSTEMS, “Photovoltaics Report,” 2012. [Online]. Available: https://www.ise.fraunhofer.de/content/dam/ise/de/documents/publications/studies/Photovoltaics-Report.pdf.

[2] F. Kessler and D. Rudmann, “Technological aspects of flexible CIGS solar cells and modules,” *Sol. Energy*, vol. 77, no. 6, pp. 685–695, 2004, doi: 10.1016/j.solener.2004.04.010.

[3] T. Kato, J. L. Wu, Y. Hirai, H. Sugimoto, and V. Bermudez, “Record Efficiency for Thin-Film Polycrystalline Solar Cells Up to 22.9% Achieved by Cs-Treated Cu(In,Ga)(Se,S)2,” *IEEE J. Photovoltaics*, vol. 9, no. 1, pp. 325–330, 2019, doi: 10.1109/JPHOTOV.2018.2882206.

[4] P. M. P. Salomé, H. Rodriguez-Alvarez, and S. Sadewasser, “Incorporation of alkali metals in chalcogenide solar cells,” *Sol. Energy Mater. Sol. Cells*, vol. 143, pp. 9–20, 2015, doi: 10.1016/j.solmat.2015.06.011.

[5] P. Jackson, R. Wuerz, D. Hariskos, E. Lotter, W. Witte, and M. Powalla, “Effects of heavy alkali elements in Cu(In,Ga)Se2 solar cells with efficiencies up to 22.6%,” *Phys. Status Solidi - Rapid Res. Lett.*, vol. 10, no. 8, pp. 583–586, 2016, doi: 10.1002/pssr.201600199.

[6] E. Avancini *et al.*, “Effects of Rubidium Fluoride and Potassium Fluoride Postdeposition Treatments on Cu(In,Ga)Se2 Thin Films and Solar Cell Performance,” *Chem. Mater.*, vol. 29, no. 22, pp. 9695–9704, 2017, doi: 10.1021/acs.chemmater.7b03412.

[7] S. Siebentritt *et al.*, “Heavy Alkali Treatment of Cu(In,Ga)Se2 Solar Cells: Surface versus Bulk Effects,” *Adv. Energy Mater.*, vol. 10, no. 8, 2020, doi: 10.1002/aenm.201903752.

[8] T. Nguyen, “Ecole Polytechnique Energy Environment Internship II Master ’ s Thesis Alternative method for depositing the absorber material of Cu (In , Ga)(S , Se) 2 solar cell,” 2018.

[9] R. Carron *et al.*, “Advanced Alkali Treatments for High-Efficiency Cu(In,Ga)Se2 Solar Cells on Flexible Substrates,” *Adv. Energy Mater.*, vol. 9, no. 24, pp. 1–8, 2019, doi: 10.1002/aenm.201900408.

[10] G. Li *et al.*, “The influence of pre-heating temperature on the CIGS thin film growth and device performance prepared in cracked-Se atmosphere,” *Semicond. Sci. Technol.*, vol. 30, no. 10, 2015, doi: 10.1088/0268-1242/30/10/105012.

[11] C. H. Huang and D. C. Wen, “The effects of annealing parameters on the crystallization and morphology of Cu(In,Ga)Se2 absorber layers prepared by annealing stacked metallic precursors,” *Int. J. Photoenergy*, vol. 2014, 2014, doi: 10.1155/2014/568648.

[12] R. Caballero, C. Guillén, M. T. Gutiérrez, and C. A. Kaufmann, “CuIn1-xGaxSe2-based thin-film solar cells by the selenization of sequentially evaporated metallic layers,” *Prog. Photovoltaics Res. Appl.*, vol. 14, no. 2, pp. 145–153, 2006, doi: 10.1002/pip.649.

[13] T. T. Wu *et al.*, “Toward high efficiency and panel size 30×40cm2 Cu(In,Ga)Se2 solar cell: Investigation of modified stacking sequences of metallic precursors and pre-annealing process without Se vapor at low temperature,” *Nano Energy*, vol. 10, pp. 28–36, 2014, doi: 10.1016/j.nanoen.2014.07.018.

[14] M. Balestrieri *et al.*, “Improving Voc with Indium and Alkali Fluorides in Cu(In,Ga)Se2 Solar Cells Deposited at Low Temperature on Polyimide,” *IEEE J. Photovoltaics*, vol. 8, no. 5, pp. 1343–1348, 2018, doi: 10.1109/JPHOTOV.2018.2857928.

[15] I. Khatri, K. Shudo, J. Matsuura, M. Sugiyama, and T. Nakada, “Impact of heat-light soaking on potassium fluoride treated CIGS solar cells with CdS buffer layer,” *Prog. Photovoltaics Res. Appl.*, vol. 26, no. 3, pp. 171–178, 2018, doi: 10.1002/pip.2962.

[16] I. Khatri, H. Fukai, H. Yamaguchi, M. Sugiyama, and T. Nakada, “Effect of potassium fluoride post-deposition treatment on Cu(In,Ga)Se2 thin films and solar cells fabricated onto sodalime glass substrates,” *Sol. Energy Mater. Sol. Cells*, vol. 155, pp. 280–287, 2016, doi: 10.1016/j.solmat.2016.06.023.

[17] P. Schöppe *et al.*, “Rubidium segregation at random grain boundaries in Cu(In,Ga)Se2 absorbers,” *Nano Energy*, vol. 42, no. October, pp. 307–313, 2017, doi: 10.1016/j.nanoen.2017.10.063.

[18] I. Pelant and J. Valenta, *Luminescence spectroscopy of semiconductors*. Oxford : Oxford university press, 2012.

[19] D. Hariskos and M. Powalla, “Thermodynamic limitations for alkali metals in Cu(In,Ga)Se2,” *J. Mater. Res.*, vol. 32, no. 20, pp. 3789–3800, 2017, doi: 10.1557/jmr.2017.394.

[20] J. Löckinger *et al.*, “The use of HfO 2 in a point contact concept for front interface passivation of Cu(In,Ga)Se 2 solar cells,” *Sol. Energy Mater. Sol. Cells*, vol. 195, no. March, pp. 213–219, 2019, doi: 10.1016/j.solmat.2019.03.009.